Quaternary International 452 (2017) 102–115

Contents lists available at ScienceDirect

Quaternary International

journal homepage: www.elsevier.com/locate/quaint

$\delta^{18}O$, $\delta^{13}C$, elemental content and depositional features of a stalagmite from Yelang Cave reflecting climate and vegetation changes since late Pleistocene in central Guizhou, China

Min Zhao [a, b], Hong-Chun Li [a, *], Chuan-Chou Shen [a, c], Su-Chen Kang [a], Chun-Yen Chou [a]

[a] Department of Geosciences, National Taiwan University, Taipei, 10617, Taiwan, ROC
[b] State Key Laboratory of Environmental Geochemistry, Institute of Geochemistry, Chinese Academy of Sciences, Guiyang, 550081, China
[c] High-Precision Mass Spectrometry and Environment Change Laboratory (HISPEC), Department of Geosciences, National Taiwan University, Taipei, 10617, Taiwan, ROC

ARTICLE INFO

Article history:
Available online 9 August 2016

Keywords:
Stalagmite
AMS ^{14}C dating
$^{230}Th/U$ dating
$\delta^{18}O$ and $\delta^{13}C$ record
Elemental content
Yelang Cave

ABSTRACT

A 13.5-cm long stalagmite from Yelang Cave in central Guizhou provides another example of AMS ^{14}C dating on stalagmites which are not suitable for $^{230}Th/U$ dating due to very low U content and low $^{230}Th/^{232}Th$ ratio. This record duplicates the published stalagmite record of 20120824-13 from the same cave (Zhao et al., 2015) not only on $\delta^{18}O$ and $\delta^{13}C$ records, but also on major growth hiatuses, facilitating speleothem $\delta^{18}O$ and $\delta^{13}C$ as climate and vegetation proxies respectively. Based on the two stalagmite records, climate and vegetation conditions can be deciphered as follow: relatively cool and dry climates with C4 dominated plants during 33.4–36 ka; very cold and dry climates with poor vegetation coverage during the Last Glacial Maximum; cold and dry climates with poor vegetation during Younger Dryas; warming and very wet climates with the best vegetation (mainly C3 plants) coverage during 9–11.5 ka BP corresponding to a maximum insolation; drying climate and decreased vegetation intensity from 9 ka to 8 ka; relatively good vegetation coverage during 5–6 ka; the summer monsoon strength decreased from 5 ka to 1.5 ka BP, but increased during the Medieval Warm Period to produce wet climates and abundant vegetation; and strongly decadal variations in moisture budget and strong deforestation due to human impact during the past 600 years. High Fe, Mn and Al contents from detritus caused dark bands near the hiatuses. Strong positive correlation of Mg and Sr with high Mg/Sr values (>23 in this study) reflects source control on the Mg and Sr variations, so that Mg/Sr is not a function of cave temperature in such a case. For pure calcite without detrital influence, Mg/Sr may register changes in cave temperature with higher Mg/Sr indicating warmer temperature. This study calls for the attention to find out climatic conditions in central Guizhou during the Bølling–Ållerød warming and the middle Holocene (6–8 ka) intervals because of lacking deposition during these intervals in Yelang Cave. Using stalagmite $\delta^{18}O$ alone to decipher climatic conditions on decadal-to-millennial scales needs to consider multiple factors such as amount, source, and temperature effects on the $\delta^{18}O$.

1. Introduction

Numerous stalagmite records from China have been used for reconstruction of paleoclimate and paleomonsoon variability (e.g., Ku and Li, 1998; Li et al., 1998, 2011a, 2011b, 2015; Wang et al., 2001, 2008; Paulsen et al., 2003; Yuan et al., 2004; Hu et al., 2008; Yin et al., 2014; Zhao et al., 2015). Taking the advantage of ICP-MS $^{230}Th/U$ dating method, stalagmite records with precise chronology have provided important information about climatic and environmental changes during the past 300 ka. For instance, the 23-ky insolation cycle has strong influence on summer monsoon intensity (e.g., Wang et al., 2008; Wan et al., 2011a). Changes in ocean circulation can affect summer monsoon variation on decadal to millennium scales (e.g., Cheng et al., 2009; Yin et al., 2014). Variations of atmospheric circulation tele-connected with ocean dynamics such as shifts of Inter-tropical Convergent Zone (ITCZ), El Niño/Southern Oscillation (ENSO) and Pacific Decadal Oscillation (PDO) can strongly alter the monsoonal rains on seasonal to decadal

* Corresponding author.
E-mail address: hcli1960@ntu.edu.tw (H.-C. Li).

http://dx.doi.org/10.1016/j.quaint.2016.07.022
1040-6182/

scales (e.g., Zhang et al., 2010; Wan et al., 2011b; Yin et al., 2014; Li et al., 2015; Zhao et al., 2015). Many stalagmite $\delta^{18}O$ records over eastern China show similar trends on millennium or longer scales (Hu et al., 2008; Wang et al., 2008; Wan et al., 2011a; Zhang et al., 2013), and many climatic events such as Younger Dryas (YD), Heinrich (H) cold events and Dansgaard–Oeschger (D–O) warming events can present in multiple stalagmite records from different caves (Ma et al., 2012; Li et al., 2014; Han et al., 2016). However, meteorological records, historical climate records and young stalagmite $\delta^{18}O$ records (<3 ky) showed strong spatial variations of summer rainfall on annual-to-decadal scales over eastern China (Qian and Lin, 2005; Tan, 2009; Zhang et al., 2010; Wan et al., 2011b; Chu et al., 2012; Yin et al., 2014; Li et al., 2015). To facilitate speleothem record as a regional rainfall and local vegetation proxy and to understand controlling factors of monsoon variability, following studies are needed: (1) age determination of young stalagmites which are not suitable for $^{230}Th/U$ dating; (2) duplicating stalagmite records from the same cave or location; (3) using both $\delta^{18}O$ and $\delta^{13}C$ as well as other proxies in the same stalagmite; and (4) comparing stalagmite record with local meteorological records and historical documents.

Many stalagmites containing very low U content (<50 ppb) and low $^{230}Th/^{232}Th$ activity ratio (<10) are not able to obtain reliable $^{230}Th/U$ dates, especially for young stalagmites (<5000 years old) due to very low radiogenic ^{230}Th counting rate. Recently, attempts of using AMS ^{14}C dating on the above mentioned stalagmites were feasible (Li et al., 2015; Zhao et al., 2015). Zhao et al. (2015) published two AMS ^{14}C-dated stalagmite records from Yelang Cave in central Guizhou and discussed the changes in climate and vegetation of the study area during the past 35 ka reflected by the $\delta^{18}O$ and $\delta^{13}C$. If this Yelang Cave record can be duplicated, it will be important for facilitating the use of AMS ^{14}C dating, $\delta^{18}O$ as rainfall proxy, and $\delta^{13}C$ as vegetation proxy in speleothem study.

This study presents a 13.6-cm long stalagmite from Yelang Cave. The stalagmite has been dated by ^{210}Pb, ICP-MS $^{230}Th/U$ and AMS ^{14}C dating methods, showing the growth periods during 33–36 ka, 7.4–13.4 ka, 4.5–6 ka, and 0–0.7 ka. A total of 750 measurements of $\delta^{18}O$ and $\delta^{13}C$ were made on the stalagmite. Some trace elemental contents have been measured throughout the stalagmite. We will compare this stalagmite record with the stalagmite 20120824-13 record from the same cave (Zhao et al., 2015) and with the dry–wetness index record reconstructed from rainfall and historic document in Guiyang (CAM, 1981; Zhang et al., 2003). The duplicated stalagmite records from Yelang Cave allow us to confirm the climatic variation and vegetation change under both natural condition and human impact in the past. The local climate conditions together with climate records from other regions will help us in understanding of variations in monsoonal climates over eastern China and their forcing factors.

2. Background information of the study area and the cave

Yelang Cave (26°2′28.00″N, 105°44′10.93″E) is located in Huangguoshu Township of Anshun City in the central Guizhou where is on the eastern edge of the Yunnan-Guizhou Plateau (Fig. 1). The cave was developed in late-to-mid Triassic limestone. Currently, about 3 km long of the cave is open to public. At the cave entrance, a lake exists due to the flowing water from the cave (Fig. 2a). From the cave entrance to inside, there is a ~1.5-km groundwater river path. Starting from the end of the river path, a 2-km land path in the cave is divided by a natural opening in the middle way (Fig. 2b). The lower part contains abundant active speleothems with many dripping water sites and pools. The upper part is relatively dry with many large and old stalagmites. Thickness of vadose zone (from cave ceiling to the surface) is generally thin (<20 m). Vegetation in the surface from the cave entrance to the lower part is dominated by C3 plants (Fig. 2a). Around the natural opening and toward to the upper part of the cave, the surface vegetation is dominated by corn (Fig. 2b). Soil in this area is rather thin with lots of bared carbonate rocks (so-called karst-desertification).

The study area is under influence of both East Asian and Indian summer monsoons with annual rainfall of 1300 mm/yr and mean temperature of 15.4 °C. Over 75% of the annual rainfall occurs from May to September (Fig. 3). Comparisons of the modern rainfall record and dry–wetness index in the study area with PDO,

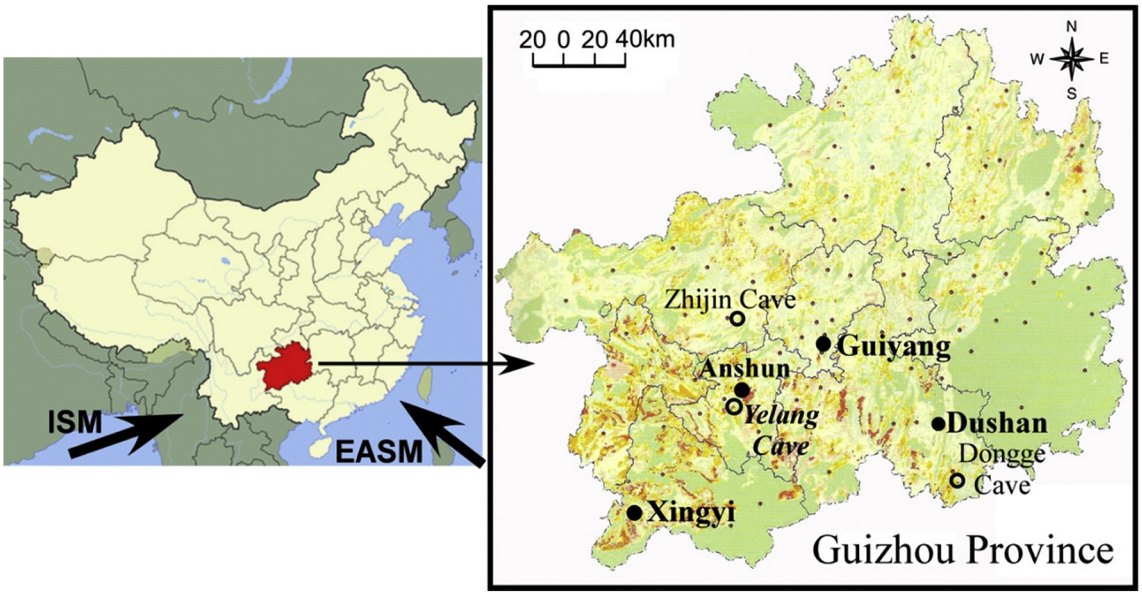

Fig. 1. The location map of study area. Left map shows the location of Guizhou in China. ISM and EASM denote Indian summer monsoon and East Asian summer monsoon, respectively. In the Guizhou map (right), the locations of Yelang Cave (Zhao et al., 2015; this study), Zhijin Cave (Kuo et al., 2011) and Dongge Cave (Yuan et al., 2004; Wang et al., 2005) are shown.

Fig. 2. a (Left) Entrance of Yelang Cave; b (Right) Surface of Yelang Cave. Building in the center is the natural opening in the mid-way of the cave.

Southern Oscillation Index (SOI) and East Asian Summer Monsoon (EASM) index indicate that wet climates were prevailing under cold PDO (La Niña condition) phase, and vice versa (Zhao et al., 2015). The rainfall variation since 1950 in the study area shows significant relationship with the Western North Pacific Monsoon (WNPM) index, but no correlation with the Indian Monsoon (IM) index (Zhao et al., 2015).

3. Stalagmite YLD-15 and analytical methods

YLD-15 is a 13.6 cm-long stalagmite from a chamber about 1500 m away from the entrance of Yelang Cave, with active dripping water on the surface (Fig. 4). The stalagmite was collected in 2008, a few meters away from the stalagmite 20120824-13 which was collected in 2012 (Zhao et al., 2015). Halving the stalagmite along the growth axis, three hiatuses at depths of 6, 8 and 9.8 cm can be identified (Fig. 4). X-ray diffraction (XRD) analyses indicate that the stalagmite contains pure calcite.

A total of 13 ^{210}Pb dating subsamples were taken from the top 12 mm with 1 mm intervals except the first two samples. ^{210}Pb activity was determined via ^{210}Po alpha-counting method with an ORTEC 576A alpha spectrometric system in the Department of Earth Sciences at the National Cheng-Kung University (NCKU) of Taiwan in 2009. The method has been described before (Li et al., 1996; Kuo et al., 2011; Zhao et al., 2015). The detection limit of this method is about 0.01 dpm/g, with relative error of 3–15% depending on counting statistics. The results are given in Table 1 and plotted in Fig. 5.

Table 1
^{210}Pb activity in stalagmite YLD-15 from Yelang Cave.

Sample	Depth (mm)	Measured ^{210}Pb (dpm/g)	Excess ^{210}Pb (dpm/g)
YLD-15-1	0.1	492.24 ± 17.61	492.17
YLD-15-2	0.2	79.07 ± 2.81	79.00
YLD-15-3	1.7 ± 0.5	7.98 ± 0.46	7.91
YLD-15-4	2.7 ± 0.5	1.10 ± 0.10	1.03
YLD-15-5	3.7 ± 0.5	1.36 ± 0.13	1.29
YLD-15-6	4.7 ± 0.5	−0.05 ± 0.01	
YLD-15-7	5.7 ± 0.5	0.33 ± 0.03	0.26
YLD-15-8	6.7 ± 0.5	0.03 ± 0.01	
YLD-15-9	7.7 ± 0.5	−0.09 ± 0.01	
YLD-15-10	8.7 ± 0.5	−0.24 ± 0.03	
YLD-15-11	9.7 ± 0.5	−0.16 ± 0.02	
YLD-15-12	10.7 ± 0.5	0.14 ± 0.01	
YLD-15-13	11.7 ± 0.5	0.09 ± 0.02	

For ^{230}Th/U dating, two batches of samples were drilled separately in 2009 (ellipse circles and black squares in Fig. 4a) (Table 2). Chemistry (Shen et al., 2003) and instrumental analysis (Shen et al., 2012; Cheng et al., 2013) were performed in the High-precision Mass Spectrometry and Environment Change Laboratory (HISPEC) at National Taiwan University (NTU) with a Neptune multi-collector inductively coupled plasma mass spectrometer (MC-ICPMS). All ^{230}Th/U dating results are listed in Table 2.

Table 2
^{230}Th/U dating results on stalagmites YLD-15.

Sampl. ID	Depth (mm)	^{238}U ppb[a]	^{232}Th ppt	δ^{234}U meas.[a]	[^{230}Th/^{238}U] activity[c]	[^{230}Th/^{232}Th] ppm[d]	Age uncorr.	Age corr.[c,e]	$\delta^{234}U_{initial}$ Corr.[b]
YLD-C-1	4–6	39.74 ± 0.24	70 ± 6.8	535 ± 19.7	0.00567 ± 0.00112	53 ± 12	404 ± 80	374 ± 85	536 ± 20
YLD-C-2	16–18	12.00 ± 0.06	24 ± 7.6	539 ± 14.9	0.00316 ± 0.00400	26 ± 35	224 ± 284	190 ± 286	539 ± 15
YLD-C-3	30–32	9.60 ± 0.03	21 ± 5.7	557 ± 14.0	0.00151 ± 0.00389	12 ± 30	106 ± 273	70 ± 276	557 ± 14
YLD-C-4	34–37	19.65 ± 34.99	24 ± 45.5	496 ± 11.4	0.00240 ± 0.00737	31 ± 99	175 ± 539	153 ± 519	496 ± 11
YLD-C-5	50–52	23.40 ± 0.09	341 ± 13.3	800 ± 15.6	0.06831 ± 0.00417	77 ± 6	4212 ± 264	3999 ± 339	809 ± 16
YLD-C-6	71–73	28.01 ± 0.09	141 ± 11.6	529 ± 9.3	0.00939 ± 0.00272	31 ± 9	673 ± 195	585 ± 214	529 ± 9
YLD-15-1A	1–3	79.37 ± 10.05	102 ± 6.8	337 ± 97.5	0.00332 ± 0.00070	42 ± 8	548 ± 143	496 ± 145	337 ± 98
YLD-15-2A	8–10	20.05 ± 0.12	61 ± 7	476 ± 11.3	0.00385 ± 0.00215	21 ± 12	285 ± 159	231 ± 168	476 ± 11
YLD-15-4A	25–27	17.56 ± 0.09	92 ± 6.9	470 ± 10.9	0.00653 ± 0.00242	20 ± 8	486 ± 181	391 ± 204	470 ± 11
YLD-15-6A	46–49	9.17 ± 13.00	10 ± 17.2	468 ± 10.2	0.00238 ± 0.00775	35 ± 119	177 ± 577	157 ± 566	468 ± 10
YLD-15-7A	56–59	31.54 ± 0.12	10,175 ± 55.7	455 ± 8.4	0.20728 ± 0.00652	11 ± 0	16,648 ± 571	10,696 ± 6166	469 ± 12
YLD-15-8A	68–70	26.75 ± 0.11	11,115 ± 182.8	696 ± 7.5	0.29711 ± 0.00961	12 ± 0	20,759 ± 737	14,217 ± 6818	724 ± 16
YLD-15-9A	76–80	37.34 ± 0.20	22,233 ± 161.6	660 ± 9.8	0.36199 ± 0.01229	10 ± 0	26,426 ± 1015	16,751 ± 10,260	692 ± 22
YLD-15-3B	94–96	41.31 ± 0.20	20,920 ± 151.3	936 ± 9.2	0.45537 ± 0.01394	15 ± 0	28651 ± 994	21,757 ± 7229	995 ± 22

Chemistry was performed on Jun. 19th, 2009 (Shen et al., 2003), and instrumental analysis on MC-ICP-MS (Shen et al., 2012). Analytical errors are 2σ of the mean.

[a] $[^{238}U] = [^{235}U] \times 137.818$ (±0.65‰) (Hiess et al., 2012); $\delta^{234}U = ([^{234}U/^{238}U]_{activity} - 1) \times 1000$.

[b] $\delta^{234}U_{initial}$ corrected was calculated based on ^{230}Th age (T), i.e., $\delta^{234}U_{initial} = \delta^{234}U_{measured} X \cdot e^{\lambda 234 * T}$, and T is corrected age.

[c] $[^{230}Th/^{238}U]_{activity} = 1 - e^{-\lambda 230 T} + (\delta^{234}U_{measured}/1000)[\lambda_{230}/(\lambda_{230} - \lambda_{234})](1 - e^{-(\lambda 230 - \lambda 234)T})$, where T is the age. Decay constants are 9.1705×10^{-6} yr^{-1} for ^{230}Th, 2.8221×10^{-6} yr^{-1} for ^{234}U (Cheng et al., 2013), and 1.55125×10^{-10} yr^{-1} for ^{238}U (Jaffey et al., 1971).

[d] The degree of detrital ^{230}Th contamination is indicated by the [^{230}Th/^{232}Th] atomic ratio instead of the activity ratio.

[e] Age corrections for samples were calculated using an estimated atomic ^{230}Th/^{232}Th ratio of 4 ± 2 ppm. Those are the values for a material at secular equilibrium, with the crustal ^{232}Th/^{238}U value of 3.8. The errors are arbitrarily assumed to be 50%.

Sixteen horizons in the stalagmite were sampled for AMS ^{14}C dating (black ellipse dots in Fig. 4b) in 2015 using a 1.0 MV Tandetron Model 4110 BO-Accelerate Mass Spectrometer (AMS) made by High Voltage Engineering Europa B.V. (HVEE) in the AMS Radiocarbon Dating Laboratory at NTU (NTUAMS Lab). Two horizons were dated twice to confirm the results. The detailed dating method was described in Zhao et al. (2015). Measured ^{14}C ages are converted to calibrated calendar ages (year BP = years before AD 1950) using CalPal Online Radiocarbon Calibration of ^{14}C (http://www.calpal-online.de/) and CALIB 7.0 (http://calib.qub.ac.uk/calib/) (Stuiver and Reimer, 1986, 1993). All AMS ^{14}C dates are listed in Table 3.

Table 3
AMS ^{14}C dating results on YLD-15.

Lab code	Sample ID	Depth (mm)	pMC (%)	$\Delta^{14}C$ (‰)	Age (a BP)	Calib. Age (a BP)
NTUAMS-893	YLD-15-16	0.1	93.11	−68.9	573 ± 2	590 ± 35
NTUAMS-892	YLD-15-15	5	95.61	−43.9	360 ± 1	410 ± 60
NTUAMS-891	YLD-15-14	11	99.57	−4.3	35 ± 0	−20 ± 10
NTUAMS-711	YLD-15-14	11	100.05	0.5	−4 ± 0	−45 ± 5
NTUAMS-710	YLD-15-13	24	85.19	−148.1	1287 ± 7	1240 ± 40
NTUAMS-709	YLD-15-12	36	79.86	−201.4	1806 ± 7	1760 ± 35
NTUAMS-708	YLD-15-11	45	76.88	−231.2	2112 ± 22	2100 ± 35
NTUAMS-890	YLD-15-10	56	92.07	−79.3	663 ± 2	620 ± 40
NTUAMS-707	YLD-15-10	56	92.79	−72.1	601 ± 2	605 ± 40
NTUAMS-706	YLD-15-9	63	59.58	−404.2	4159 ± 11	4730 ± 70
NTUAMS-757	YLD-15-8	78	54.01	−459.9	4948 ± 21	5680 ± 35
NTUAMS-756	YLD-15-7	87	32.67	−673.3	8986 ± 40	10,125 ± 90
NTUAMS-755	YLD-15-6	94	27.52	−724.8	10,363 ± 62	12,290 ± 195
NTUAMS-754	YLD-15-5	98	2.46	−975.4	29,766 ± 480	33,960 ± 440
NTUAMS-753	YLD-15-4	107	2.74	−972.6	28,903 ± 363	33,365 ± 470
NTUAMS-752	YLD-15-3	115	2.05	−979.5	31,245 ± 773	35,540 ± 835
NTUAMS-751	YLD-15-2	127	1.94	−980.6	31,678 ± 662	35,990 ± 970
NTUAMS-750	YLD-15-1	131	2.17	−978.3	30,765 ± 752	35,050 ± 690

A total of 750 samples for $\delta^{18}O$ and $\delta^{13}C$ analyses were milled along the growth axis of YLD-15, with the sampling resolutions at an interval of 0.1 mm from top to 20 mm and an interval of 0.2 mm from 20.2 mm to the bottom of 135 mm (rectangles in Fig. 4). Stable isotope analyses were done on a Finnigan MAT-253 isotopic ratio mass spectrometer (IRMS) equipped with a Kiel-III Carbonate Device in the Department of Geosciences, NTU. $\delta^{18}O$ and $\delta^{13}C$ values are reported relative to the Vienna Pee Dee Belemnite (VPDB) standard at 25 °C. The standard deviations of an international standard, NBS-19, runs are normally 0.08‰ for $\delta^{18}O$ and 0.06‰ for $\delta^{13}C$. A working standard, MAB (a pure marble formed in Taroko National Park of Eastern Taiwan ca. 250 million years ago with $\delta^{18}O = -6.9‰$ and $\delta^{13}C = 3.4‰$), was measured after every 5–7 sample measurements to monitor any instrumental drift. The $\delta^{18}O$ and $\delta^{13}C$ results are plotted in Fig. 4.

Samples for elemental content analyses were combined from powder samples for stable isotope analyses. Since ~2 mL solution at >1 ppb concentration level is needed for measurement of each element using an inductively coupled plasma atomic emission spectroscopy (ICP-OES) (Olesik, 1991), we combined several samples from adjacent depths. Therefore, the sample depth is the mean depth of the combined sample depths. The weighted sample was dissolved with 1 mL concentrated HNO_3 and 1 mL H_2O_2, then diluted with deionized water to 20 mL. The solution was used for measurement of elemental concentration with Perkin Elmer (PE) Optima 2100 DV ICP-OES in the Department of Earth Sciences at NCKU. In this study, we measured 6 elements including Mg, Sr, Al, Fe, Mn, and Zn. The measured concentrations contain generally a relative standard deviation (RSD) of <2%. All results are listed in Table 5.

Table 4
Ages for Stal-Age modeling.

Sample ID	Depth (mm)	Age (yr BP)	Error (±)	Method
	0	−58	3	^{210}Pb, ^{14}C
YLD-15-14	11	−45	5	^{14}C
YLD-C-2	17	190	286	U–Th
YLD-15-4A	26	391	204	U–Th
YLD-C-3	31	70	276	U–Th
YLD-C-4	35.5	153	519	U–Th
YLD-15-6A	47.5	157	566	U–Th
YLD-15-10	56	615	40	^{14}C
YLD-C-5	57	3999	339	U–Th
YLD-15-7A	61	10,696	6166	U–Th
YLD-15-9	63	4730	70	^{14}C
YLD-15-8	78	5680	35	^{14}C
YLD-15-9A	78	16,751	10,260	U–Th
YLD-15-7	87	10,125	90	^{14}C
YLD-15-6	94	12,290	195	^{14}C
YLD-15-3B	95	21,757	7229	U–Th
YLD-15-5	98	33,960	440	^{14}C
YLD-15-4	107	33,365	470	^{14}C
YLD-15-3	115	35,540	835	^{14}C
YLD-15-2	127	35,990	970	^{14}C
YLD-15-1	131	35,050	690	^{14}C

4. Results and discussions

4.1. Chronology

Stalagmite YLD-15 was active in growth position during collection. Therefore, the first attempt of chronological determination was using ^{210}Pb method to find out a brief growth rate. Then, we used $^{230}Th/U$ dating for age determination in 2009. However, the $^{230}Th/U$ dating results did not allow us to obtain a reliable chronology. Thus, we conducted AMS ^{14}C dating on the stalagmite in 2015. We shall discuss all results of each dating methods and determine the correct chronology of the stalagmite below.

4.1.1. ^{210}Pb dating

Table 1 lists ^{210}Pb activity of the samples. The first sample was scratched from the stalagmite surface, so that it may contain detritus from soil above the cave and/or dust inside the cave brought by tourists. This sample contains extremely high ^{210}Pb activity, being 492 dpm/g. The second sample which also contains very high ^{210}Pb activity (79 dpm/g) was scratched from the same spot after the first sample. Although we do not know the real reason for the high ^{210}Pb activities in these two samples, the initial ^{210}Pb activity in the source must be changed which means that the two samples do not meet the assumption of ^{210}Pb dating (constant initial ^{210}Pb activity from source). Therefore, we do not include these two data points for excess ^{210}Pb activity fitting.

Samples below 4.7 mm depth of stalagmite have very low ^{210}Pb activity due to low U contents. The ^{210}Pb activities of samples at 4.7, 7.7, 8.7, 9.7 mm depths are lower than the background of the counting system, which means that the supported ^{210}Pb activities are below detection limit. If we use the average value of the positive ^{210}Pb activities below 4.7 mm as the supported ^{210}Pb activity, being 0.148 dpm/g, this value is significantly higher than the ^{210}Pb activities at several depths below 4.7 mm. Thus, we take the ^{210}Pb activity values below 5.7 mm depth as supported ^{210}Pb activity, which yields an average value of 0.07 dpm/g. Using total ^{210}Pb activity minus this average value, we obtain excess ^{210}Pb activity at each depth (Table 1). Fig. 5 shows the exponential decay of excess ^{210}Pb in the stalagmite excluding the two top samples. Based on the fitting of excess ^{210}Pb decay trend, an average growth rate of 0.0323 mm/yr is resulted. The ^{210}Pb dating result indicates that the top 6.7 mm of YLD-15 should be younger than 120 years. However,

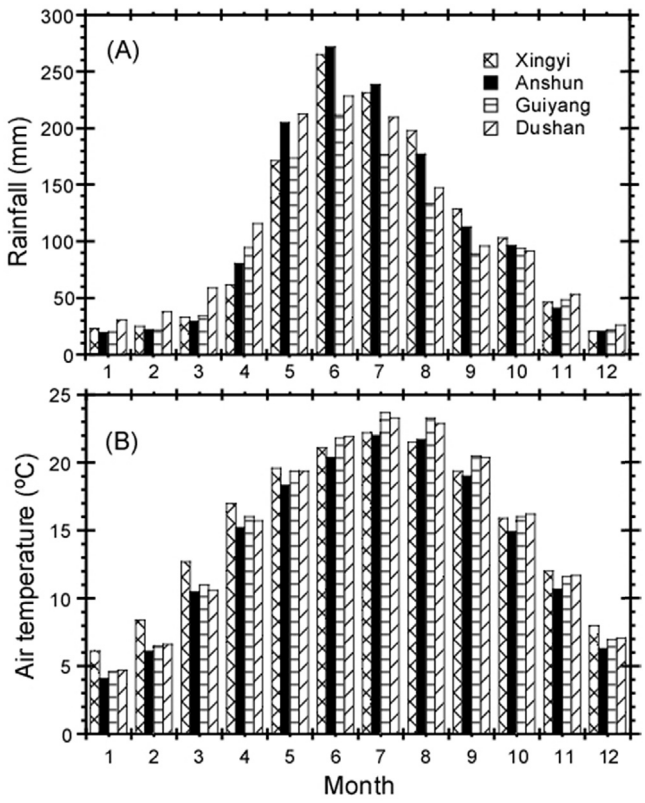

Fig. 3. Monthly rainfall and air temperature of the study area (Zhao et al., 2015).

the age at 7 mm depth being older than 120 years is not supported by AMS ^{14}C dating (Table 3). Two AMS ^{14}C dates at depth of 11 mm show "nuclear bomb ^{14}C signal", reflecting the deposition of the calcite above this depth should be after AD 1950. Therefore, the growth rate of 0.0323 mm/yr given by the ^{210}Pb dating should be underestimated. Note that if the two top points in Table 1 were included in Fig. 5, the growth rate would be even smaller. Similar situation would occur if we put the supported ^{210}Pb activity starting from 4.7 mm depth and downward. Nevertheless, the ^{210}Pb dating results only illustrate that the surface of YLD-15 is modern.

4.1.2. ^{230}Th dating

Fourteen ^{230}Th/U dates in Table 2 have large uncertainties and are lack of stratigraphic orders due to very low U contents. Although the ^{230}Th/U ages have large uncertainties, eight ^{230}Th/U dates in the upper 5.2 cm part are younger than 800 years which agree with the AMS ^{14}C results (Fig. 4). This section of the stalagmite has relatively pure calcite with white color, and both U and Th contents are very low (Table 2), which agree with very low supported ^{210}Pb activity. The part of YLD-15 below the first hiatus at 6 cm depth contains ^{230}Th/U ages in late Pleistocene within 30,000 years (Fig. 4). It is obvious that the ^{230}Th/U dating results are not able to reconstruct chronology of the stalagmite besides to give the age ranges.

4.1.3. AMS ^{14}C dating and chronology of YLD-15

Because of dead carbon fraction (DCF) influence during the carbonate precipitation, AMS ^{14}C dating is generally not considered for stalagmite dating. However, recent studies have shown that DCF in some stalagmites are relatively constant through time, and some stalagmites contain "the nuclear bomb C curve" (Beck et al., 2001; Genty et al., 2001; Hoffmann et al., 2010; Oster et al., 2010; Southon et al., 2012). The AMS ^{14}C dating results of stalagmites 20120824-13 and 20120824-11 from Yelang Cave were successfully used for constructing stalagmite chronology (Zhao et al., 2015). Li et al. (2015) found out when CO_2 exchange between dissolved inorganic carbon (DIC) in seepage water and atmospheric CO_2 in the vadose zone and inside the cave, the DCF influence may be minimal though DCF would affect δ^{13}C strongly. In such a circumstance, AMS ^{14}C dating on such a stalagmite may provide correct chronology. In order to find out ^{14}C ages with minimal DCF influence, a series of ^{14}C dating samples should be made at different depths in a stalagmite. When a ^{14}C age of an upper layer sample is older than that of lower layer sample, this ^{14}C age contains significant DCF influence and should be removed for chronological fitting. In so doing, a batch of ^{14}C ages which have minimal DCF influence may be used to build up the stalagmite chronology.

Table 3 lists all AMS ^{14}C ages in stalagmite YLD-15. Except the ^{14}C ages in the upper 5.6 cm part, the rest ^{14}C ages are in stratigraphic sequence (Fig. 4b). For the upper 5.6 cm part, the ^{14}C ages at depths of 1.1 cm and 5.6 cm have minimal DCF influence. These layers were dated twice to make sure that the ages are correct

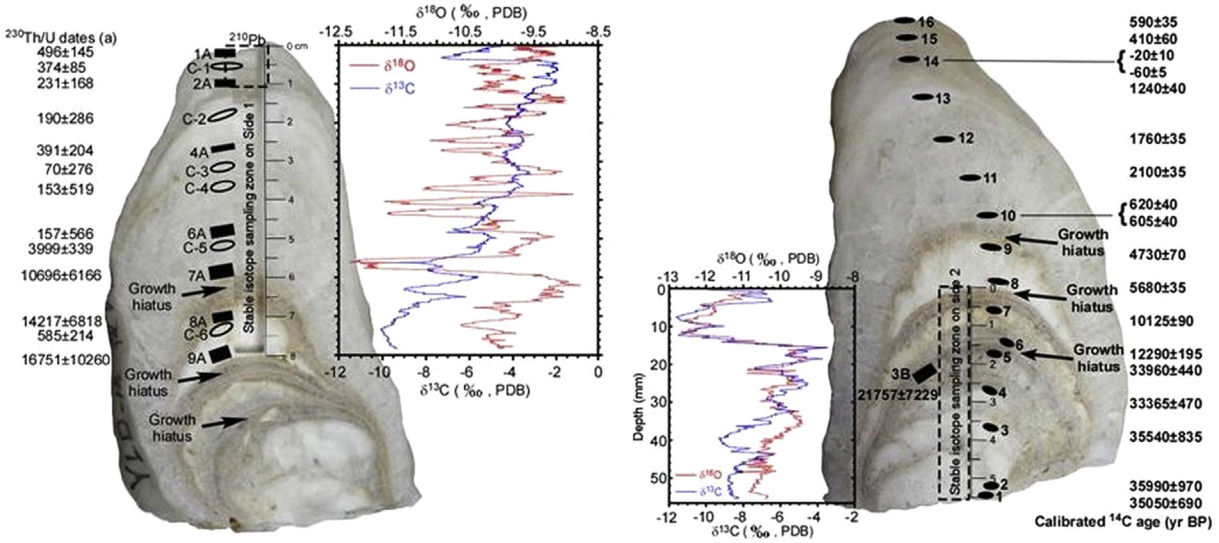

Fig. 4. Picture of Stalagmite YLD-15 with ^{230}Th/U dates, AMS ^{14}C dates as well as δ^{18}O and δ^{13}C records. Left: Side 1; Right: Side 2.

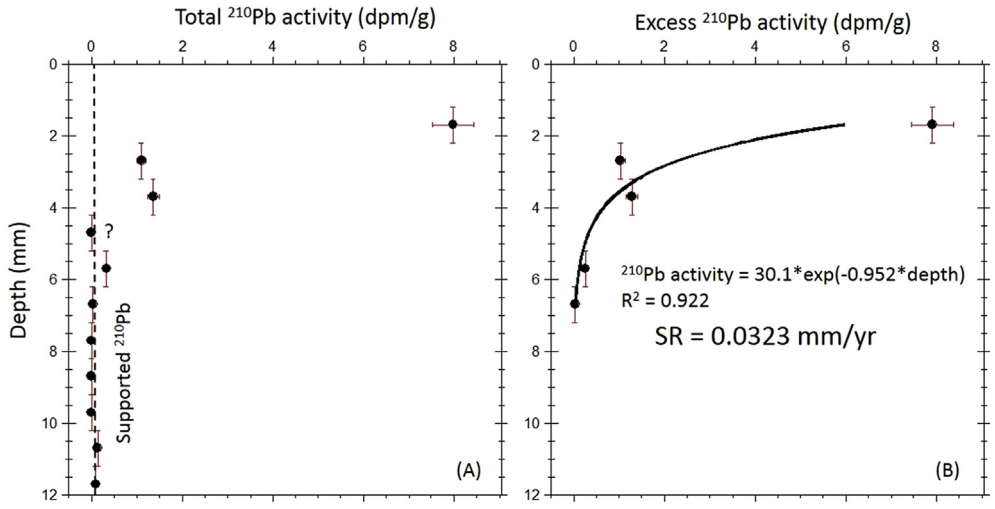

Fig. 5. ^{210}Pb dating profiles of Stalagmite YLD-15. (A) Total ^{210}Pb activity; (B) Excess ^{210}Pb activity.

(Table 3). Since other ^{14}C ages in this part are significantly influenced by DCF, we have only dates at 1.1 cm and 5.6 cm depths as well as the surface (AD 2009 = −59 a BP) for age–depth correlation in this part. The fitting yields a linear relationship of age (a BP) = −132 + 13.136*depth (mm) (R^2 = 0.98), giving a growth rate of 0.076 mm/yr. We admit that this chronology is not perfect. The ^{210}Pb dating and ^{230}Th/U dating results generally support this chronology. In the next section, we will use Stal-Age program (an algorithm similar to Bayesian approach) and ages from three dating methods to calculate the chronology for comparison.

For the ^{14}C ages below 5.6 cm depth, we do not know how much DCF influence exists in each age. However, the ^{14}C ages generally agree with the ^{230}Th/U dates even though the latter ones have very large uncertainties. Based on the ^{14}C dating results, there are four different growth periods in YLD-15: (1) the upper 6-cm, transparent and pure calcite grew continuously during the past 660 years. (2) From 6.7 cm to 8 cm, white but non-transparent zone formed between 4500 and 5700 yr BP. (3) From 8.2 to 9.8 cm, light brown (in the web version) layer deposited between 10,100 and 12,300 yr BP. (4) From 9.8 cm to the bottom of the stalagmite, age ranges from 33,400 to 36,000 yr BP (Fig. 4b).

4.1.4. STAL-AGE modeling of YLD-15 chronology

Scholz and Hoffmann (2011) developed an algorithm, so-called Stal-Age, for constructing speleothem age models. According to the program design, Stal-Age can deal with stalagmites which have age outliers, inversions, hiatuses and large changes in growth rate. Here we use 21 ages and their uncertainties to put in Stal-Age model (Table 4). The modeled chronology is plotted in Fig. 6a. For coarse resolution, the modeled chronology is similar to the chronology that is based on AMS ^{14}C dates only discussed in Section 4.1.3 (Fig. 6b). However, when we enlarge each segments, significant difference exists between two chronologies for the youngest part (Fig. 7a). The Stal-Age modeled chronology has two apparent mistakes: (1) showing continuous ages at hiatuses; and (2) giving impossible ages for the top 11-mm part. The stalagmite was collected in 2009 (−59 yr BP), so that no age should be younger than that. Therefore, we have to use "Stal-Age plus" chronology for the top 11-mm part instead of "Stal-Age" chronology (Fig. 7a). Also, for the upper 60-mm part, the Stal-Age modeled chronology resulted in very unreasonable growth rates (Fig. 7a). For depths from 60 mm to 94 mm of YLD-15, the two chronologies are almost identical (Fig. 7b and c). However, the ages between 94 mm and 98 mm depths given by the Stal-Age modeled chronology are much older than that calculated from the AMS ^{14}C dates. This is because the poor ^{230}Th/U age at 95 mm depth influences the modeling result. And, the hiatus around 98 mm depth indicates that no

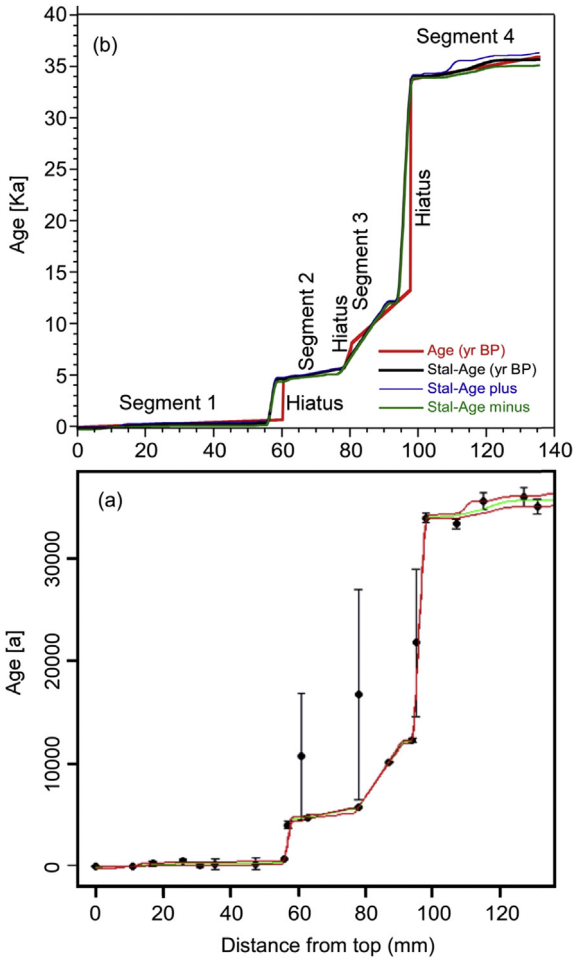

Fig. 6. Chronology construction of YLD-15. (a) Stal-Age modeled chronology based on AMS ^{14}C dates and ^{230}Th/U dates in Table 4. (b) Comparison of the Stal-Age modeled chronology with the Age–depth relationship of YLD-15 based on AMS ^{14}C chronology.

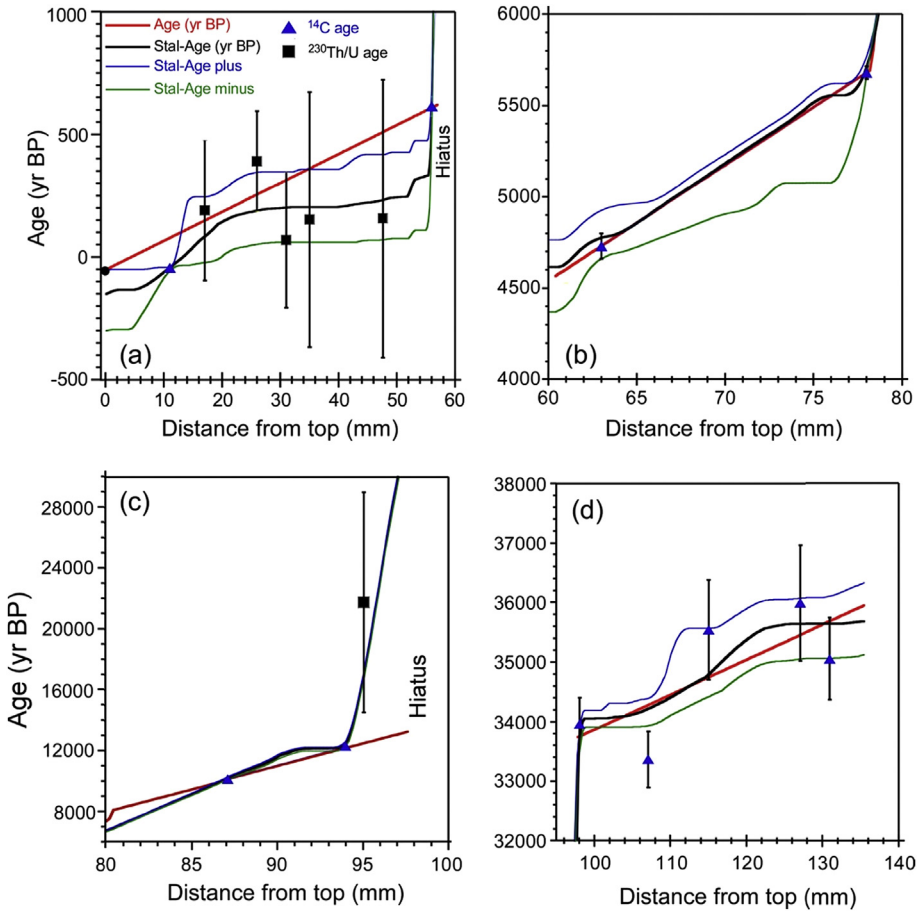

Fig. 7. Detailed evaluation of YLD-15 chronologies. (a) Segment 0–60 mm; (b) Segment 60–80 mm; (c) Segment 80–96 mm; and (d) Segment 96–136 mm.

deposition occurred between 13 ka BP and 33 ka BP. The ages determined by the Stal-Age modeled chronology between 94 mm and 98 mm are not reasonable. For the oldest segment of YLD-15, the two chronologies are similar within uncertainty (Fig. 7d). Since we will not discuss high-resolution temporal variations of the $\delta^{18}O$ and $\delta^{13}C$ records during this period, using either chronology will not make difference in isotopic interpretation. In summary, because of the Stal-Age modeled chronology of YLD-15 is not better than the chronology determined by the AMS ^{14}C ages described in Section 4.1.3, we do not adopt the Stal-Age modeled chronology.

In the following sections, the comparisons of YLD-15 record with Dry–wetness index reconstructed from rainfall and historic documents and with Stalagmite 20120824-13 record from the same cave shall demonstrate that the chronology of YLD-15 determined by the AMS ^{14}C ages is acceptable. In contrast, the Stal-Age modeled chronology for the youngest segment of YLD-15 is not acceptable.

4.2. $\delta^{18}O$ and $\delta^{13}C$ records of YLD-15

The YLD-15 record has $\delta^{18}O$ and $\delta^{13}C$ values ranging from −12.68‰ to −8.74‰ with an average −10.19‰ and from −11.6‰ to −1.9‰ with an average −6.00‰, respectively. Since the criterions of Hendy Test (Hendy, 1971) which was the classic way to detect isotopic disequilibrium, has been questioned by many recent studies (Fairchild et al., 2006; Dorale and Liu, 2009; Zhang et al., 2013; Yin et al., 2014; Li et al., 2015), we do not perform Hendy Test. It is generally agreed that duplicate $\delta^{18}O$ records from the same cave is the best evidence of $\delta^{18}O$ as a climatic proxy. In addition, Dorale and Liu (2009) suggested that co-variance of $\delta^{18}O$ and $\delta^{13}C$ in a stalagmite could be an illustration of isotopic equilibrium fractionation. Stalagmites YLD-15 and 20120824-13 were taken from nearby locations in the same cave. Fig. 8 shows the comparison of overlapping period in the two records which have independent age controls. First of all, the $\delta^{18}O$ and $\delta^{13}C$ records based on the Stal-Age modeled chronology are not comparable to the 20120824-13 records (Fig. 8). Stal-Age modeling approach does not provide correct chronology for the youngest part of YLD-15 because the five poor $^{230}Th/U$ dates have strong influence on the modeling result. We should compare the two stalagmite records with the chronology determined by AMS ^{14}C dates (plot (A) vs. plot (B) and plot (D) vs. (E) in Fig. 8). Although the $\delta^{18}O$ records of the two stalagmites do not match prior to AD 1700 due to age uncertainty, the major features in both $\delta^{18}O$ records are comparable. For the $\delta^{13}C$ records, the increasing trend from AD 1400–1950 and the decreasing trend after 1940 are similar. It seems that the peaks Q and N-M in the $\delta^{13}C$ records of both stalagmite should match. If we shift the $\delta^{13}C$ peaks Q and N-M of YLD-15 to younger ages to match these in the 20120824-13 record, then their $\delta^{18}O$ peaks can compare better. Whether the YLD-15 record prior to AD 1700 should move toward younger age, or the 20120824-13 record should move to older age? We will compare the record with Dry–wetness index reconstructed from rainfall and historic documents which has accurate age control. Nevertheless, the similarities of $\delta^{18}O$ and $\delta^{13}C$ records in the two stalagmites serve as evidence that these two stalagmite records can reflect local climate and vegetation changes.

It is commonly accepted that rainfall amount is the dominant factor to influence stalagmite $\delta^{18}O$ on annual-to-decadal scales in

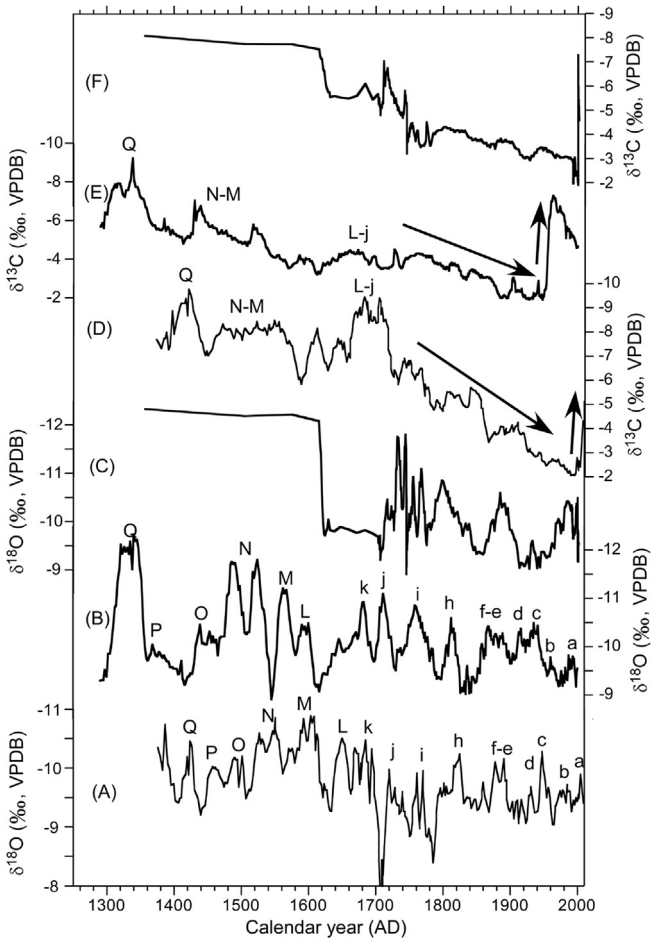

Fig. 8. Comparisons of the $\delta^{18}O$ and $\delta^{13}C$ records of YLD-15 with the $\delta^{18}O$ and $\delta^{13}C$ records of 20120824-13 (Zhao et al., 2015) during the last 700 years. (A) and (D) $\delta^{18}O$ and $\delta^{13}C$ of 20120824-13; (B) and (E) $\delta^{18}O$ and $\delta^{13}C$ of YLD-15 based on AMS ^{14}C chronology; and (C) and (F) $\delta^{18}O$ of and $\delta^{13}C$ of YLD-15 based on the Stal-Age modeled chronology.

monsoonal regions (Li et al., 1998, 2011a, 2011b, 2015; Wan et al., 2011a,b; Yin et al., 2014; Zhao et al., 2015). Here we use rainfall record of Guiyang and Dry–Wetness index (DWI) record of South China which have exactly age control to compare with the stalagmite $\delta^{18}O$ (Fig. 9). Since the chronology of YLD-15 has large uncertainty on interannual-to-decadal scales, we focus on the comparison on inter-decadal scales. The DWI record (Zhang et al., 2003, 2010 and references therein) and the rainfall record are 5-yr running average. In the DWI record, at least 16 wet–dry episodes (letters in Fig. 9) on decadal scales during the 500 years can be clearly identified. The $\delta^{18}O$ record of YLD-15 exhibits corresponding changes within age uncertainty, a heavy $\delta^{18}O$ swing corresponding to a dry episode; and vice versa (Fig. 9). The comparison is better for post AD 1700 period. If the record of YLD-15 prior to AD 1700 moves toward younger ages, the comparison is more reasonable (i.e., Capital letters in the YLD-15 record match with letters in the DWI record). This shift agrees with the interpretation of the comparison between the YLD-15 record and 20120824-13 record (Fig. 8). The present comparison illustrates not only that the $\delta^{18}O$ record reflects wetness change in Yelang Cave, but also that the chronology of YLD-15 is reasonable. Again, this comparison does not support the Stal-Age modeled chronology for the youngest part of YLD-15 record.

4.3. Stalagmite elemental records

Variations of elemental contents in a stalagmite may provide changes in soil condition, dissolution/precipitation of carbonate in vadose zone, water temperature, and others (Fairchild and Treble, 2009; Li et al., 2015). Elemental contents in stalagmites come from three sources: dissolved elements in source water co-precipitated with carbonate, particles in drip water derived from the surface above the cave, and dusts inside the cave. In this study, we analyze concentrations of Mg, Sr, Fe, Mn, Zn, Al, and calculate Mg/Sr ratio throughout YLD-15, but focus on the color changed zones. Fig. 10 displays comparisons among the trace element concentration, stratigraphic feature, $\delta^{18}O$ and $\delta^{13}C$ records.

The first apparent feature of the elemental contents is that Fe and Mn have a strongly positive correlation ($R^2 = 0.824$), indicating that they have the same source and similar behavior. All three dark layers at the hiatuses have high Fe and Mn contents (Fig. 10), perhaps due to Fe oxides and Mn oxides in the detritus. In general, surface water contains very low Fe and Mn concentrations, and dissolved Fe^{2+} and Mn^{2+} exist mainly under reduced conditions. Hence, it is unlikely that the high Fe and Mn peaks were caused by dissolved Fe and Mn in source water. Instead, the high Fe and Mn at 6.7, 8.02 and 9.8 cm depths can be explained by high detrital contents either carried by water or dust fall during the growth hiatuses of the stalagmite. Al contents were also high at these three dark layers, supporting above explanation. In addition, the $\delta^{13}C$ had positive excursions corresponding to the Al and Fe peaks around the hiatuses, reflecting increased $\delta^{13}C$ of soil CO_2 which might be caused by vegetation decline under dry climates. Besides these three dark layers, Fe and Mn contents are also significantly high at 0.3 mm and 25.5 mm depths where no hiatus and dark color can be observed (Fig. 10). High Fe and Mn contents at these two depths might come from dissolved Fe and Mn in the source water as detrital content is negligible in the upper part. Currently, the reason of the high Fe and Mn remains unclear. It is interesting to see that Al content has the lowest level between 3.3 cm and 5.6 cm depths (AD 1300–1600) in the stalagmite (Fig. 10). This period is the first half of Little Ice Age (LIA) (Yin et al., 2014 and reference therein). This segment contains very pure calcite, so that Al should come from dissolved Al in the source water. The lower Al contents during this period might be due to cold but relatively wet climates.

Mg and Sr as well as Mg/Sr ratio in stalagmites have been used for deciphering cave temperature and prior carbonate precipitation (PCP) process (Fairchild et al., 2000, 2006; Huang and Fairchild, 2001; Ma et al., 2002; Johnson et al., 2006; Li et al., 2006). Because the primary source of dissolved (vs. detrital phase) trace elements in speleothems comes from dissolution of rocks in the overlying regolith and bedrock carbonates through the vadose zone (Fairchild et al., 2006), Mg and Sr may have similar source and behavior in a cave system. Previous studies have shown a positive temperature coefficient in the distribution of Mg between calcite and water ($D_{Mg/Ca}$) (Katz, 1973; Fuchtbauer and Hardie, 1976; Gascoyne, 1983), opening the possibility of assessing the past changes in cave temperature which reflects mean annual temperature above the cave using speleothem deposits (Gascoyne, 1983; Goede and Vogel, 1991). To correct for any change of Mg/Ca in the source water, the use of Sr/Ca was suggested (Goede and Vogel, 1991), as this ratio is temperature dependent in the calcite formation (Kinsman and Holland, 1969; Katz et al., 1972; Gascoyne, 1983). However, in order to use Mg/Sr in a stalagmite as a temperature proxy, the stalagmite should be pure calcite, meaning that the contribution of Mg and Sr from detrital phase is negligible. Another factor affecting Mg/Ca and Sr/Ca ratios is carbonate precipitation in vadose zone prior to the seepage water entering the cave, so called

PCP. Therefore, the use of stalagmite Mg/Sr as a temperature proxy has not been accepted commonly yet.

In YLD-15, Mg content is one order magnitude higher than Sr content (Table 5). Although Mg and Sr have similar trends, the variation trends are different in two segments: 0–6 cm and 6–13.5 cm (Fig. 11A). The relationships in these two segments are different (Fig. 11B). In the older (lower) segment, Mg contents are relatively higher with Mg/Sr generally greater than 23 (Fig. 11A). Mg and Sr in this segment have strongly positive correlation ($R^2 = 0.974$), excluding the two low Mg/Sr points (Fig. 11B). This strong correlation may indicate that changes of Mg and Sr were mainly controlled by source variation. Therefore, the Mg/Sr ratios (>23) may not reflect cave temperature change. Three data points (at 0.3, 8.5 and 20.6 mm depths) in the younger (upper) segment seem to fall on the linear correlation (Fig. 11B), which may also contain detrital influence. Except these three points, Mg/Sr ratios in the younger (upper) segment are less than 20 accompanied with low Mg, Fe, Mn and Al contents. The calcite in this segment is very pure. Therefore, the Mg/Sr ratio may reflect temperature change, with higher Mg/Sr indicating warmer temperature; and vice versa. During the past 600 years or so, the Mg/Sr values were lower in the first half of LIA (ca. AD 1250–1550), reflecting colder conditions. Mg/Sr slightly in creased afterwards.

5. Interpretation of YLD-15 record

Fig. 12 shows the entire $\delta^{18}O$ and $\delta^{13}C$ records of stalagmite YLD-15. For the long-term variations, $\delta^{18}O$ and $\delta^{13}C$ vary in the same direction, being lighter $\delta^{13}C$ excursion corresponding to lighter $\delta^{18}O$ swing. The co-variance indicates that the $\delta^{18}O$ and $\delta^{13}C$ records reflect climate and vegetation changes (Dorale and Liu, 2009), better vegetation development (lighter $\delta^{13}C$) under wetter climatic condition (lighter $\delta^{18}O$). Based on the chronology that should be good on decadal-to-centennial scales, the four growth periods have three overlapping periods with Stalagmite 20120824-13 published by Zhao et al. (2015): episode during Marine Isotope Stage 3 (MIS3), early Holocene (8–13 ka) and the past 700 years. Both records have growth hiatuses during 13.5–31 ka and 6–8 ka. YLD-15 had deposition between 4.5 ka and 5.8 ka, whereas 20120824-13 had growth between 0.7 ka and 4.5 ka. The frequent growth gaps may reflect thin overlying vadose zone at the stalagmite site, so that the calcite deposition can sensitively respond to the surface change.

5.1. Climate and vegetation condition during 33–36 ka

From 9.8 cm to the bottom (from 33,400 to 36,000 y BP) of YLD-15, the $\delta^{18}O$ and $\delta^{13}C$ were −11.21‰ to −9.30‰ with an average value of −10.17‰ and −9.32‰ to −3.76‰ with an average value of −7.18‰, respectively. This growth period was between Heinrich event 3 (ca. 31 ka) and 4 (ca. 38 ka) (Hemming, 2004). The $\delta^{13}C$ values from around −8‰ in the early time increased to about −4‰ at the end of this period, indicating gradually decline of vegetation intensity due to drying and cooling climatic conditions. Although growth hiatus appeared during the Last Glacial Maximum (LGM),

Table 5
Elemental contents of the stalagmite.

Sample ID	Depth (mm)	Mg (mg/kg)	Sr (mg/kg)	Al (mg/kg)	Fe (mg/kg)	Mn (mg/kg)	Zn (mg/kg)	Mg/Sr
YLD-15-003	0.3	652.69	20.12	202.80	77.69	4.67	9.74	32.44
YLD-15-85	8.5	822.12	33.61	190.96	9.25	1.31	4.86	24.46
YLD-15-114	11.4	610.20	36.52	181.07	6.99	1.31	6.44	16.71
YLD-15-143	14.5	646.50	39.64	185.65	5.58	1.16	2.00	16.31
YLD-15-160	16.0	534.41	38.02	183.92	2.96	1.10	1.90	14.06
YLD-15-173	17.3	537.25	34.46	177.55	2.90	1.03	2.01	15.59
YLD-15-203	20.6	505.29	21.15	174.52	1.38	0.94	3.09	23.89
YLD-15-215	23.0	504.74	31.93	184.59	2.04	1.01	6.71	15.81
YLD-15-223	24.6	639.64	37.00	177.43	2.13	0.86	0.49	17.29
YLD-15-229	25.8	539.40	33.59	187.91	41.75	1.46	0.81	16.06
YLD-15-236	27.2	588.76	34.87	191.40	3.10	1.08	1.63	16.88
YLD-15-263	32.6	578.26	30.37	176.52	1.09	0.77	1.01	19.04
YLD-15-286	37.2	463.77	31.10	133.98	2.15	0.49	0.40	14.91
YLD-15-293	38.6	435.17	28.35	135.89	1.79	0.54	0.83	15.35
YLD-15-302	40.4	350.47	35.47	141.94	3.51	0.47	0.79	9.88
YLD-15-309	41.8	404.91	31.88	137.14	2.05	0.41	0.60	12.70
YLD-15-318	43.6	404.17	32.21	133.46	1.67	0.60	1.63	12.55
YLD-15-348	49.6	452.98	35.00	142.36	3.96	0.51	1.91	12.94
YLD-15-380	56.0	387.50	29.20	142.92	6.48	0.58	1.83	13.27
YLD-15-410	62.0	610.00	41.63	149.93	2.34	0.57	0.66	14.65
YLD-15-439	67.8	640.59	23.83	208.86	43.74	6.70	2.68	26.89
YLD-15-462	72.4	560.00	20.38	173.32	8.64	1.93	2.06	27.48
YLD-15-501	80.9	720.43	27.05	285.58	90.30	10.71	5.57	26.63
YLD-15-531	88.4	561.08	22.63	190.88	13.74	1.93	2.45	24.80
YLD-15-564	97.5	934.13	36.73	272.22	64.33	8.20	3.74	25.43
YLD-15-593	101.7	824.18	48.48	198.24	8.50	1.16	8.84	17.00
YLD-15-642	112.3	1561.64	52.12	175.17	12.18	1.75	1.56	29.96
YLD-15-650	114.0	1240.38	42.92	181.22	8.35	1.23	1.80	28.90
YLD-15-692	123.0	796.92	37.36	165.92	11.93	1.10	2.54	21.33
YLD-15-716	128.2	1015.87	38.07	180.04	5.35	0.95	1.84	26.69
YLD-15-747	134.8	1090.10	36.05	198.13	8.70	1.31	6.50	30.24

In summary, high Fe, Mn and Al contents reflect detrital influence, resulting in dark bands caused by dry climatic conditions. Strong positive Mg–Sr correlation with higher Mg/Sr reflects source impact on Mg and Sr changes. In such a circumstance, Mg/Sr is not a function of cave temperature. For pure calcite, Mg/Sr variation may reflect cave temperature change with higher ratio indicating warmer condition.

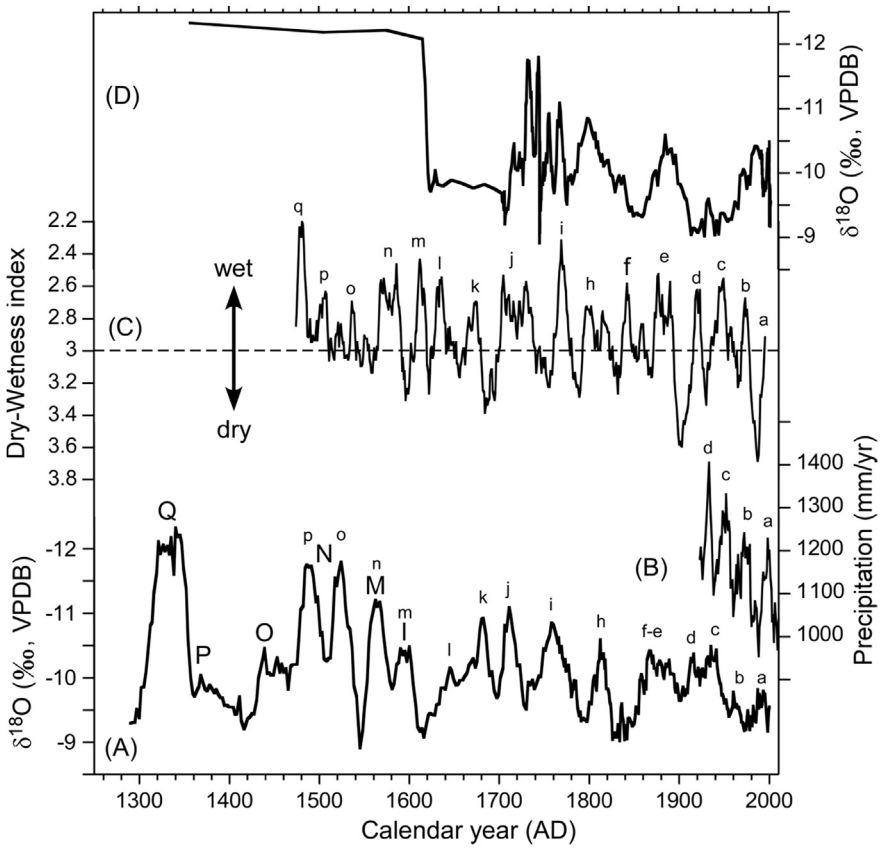

Fig. 9. Comparison of the $\delta^{18}O$ record of YLD-15 with Guiyang rainfall record (Data from http://cdc.cma.gov.cn) and Dry–Wetness index record (CAM, 1981; Zhang et al., 2003). Letters denote wet episodes.

we anticipate that climate during the LGM must be cold and dry in the study area which caused the growth hiatuses at LGM in both YLD-15 and 20120824-13.

5.2. Climate and vegetation during 4.5–13.3 ka

Three growth hiatuses in YLD-15 occurred at 6, 8 and 9.8 cm depths corresponding to the gaps of 0.7–4.5 ka, 6–7.6 ka and 13.4–33.4 ka, respectively. From 8 cm to 9.7 cm (7.4–13.4 ka), the record contains Younger Dryas (YD) and Holocene Optimum (HO), similar to the 20120824-13 record. Both $\delta^{18}O$ and $\delta^{13}C$ values became very heavy around 12.5 ka, reflecting dry climate and poor vegetation development during the YD interval (Fig. 12). During early Holocene (11.5–8 ka), the $\delta^{18}O$ decreased to a minimum value of −12.68‰ at 11.5 ka, and kept relatively light until 9 ka before starting to increase continuously (Fig. 12). The $\delta^{13}C$ values were also lightest in the entire record, suggest abundant vegetation with trees and shrubs (C3 plants) corresponding to wet and cool climatic conditions. Many Chinese stalagmite records show that very strong summer monsoon intensity corresponding to a maximum solar irradiation (i.e., insolation) occurred during the Holocene Optimum (Dykoski et al., 2005; Hu et al., 2008; Wan et al., 2011a; Zhang et al., 2013; Zhao et al., 2015). However, unlike the Dongge record which shows that the strong summer monsoon intensity lasted until 6 ka before started to decrease (Dykoski et al., 2005; Wang et al., 2005), both YLD-15 and 20120824-13 from Yelang Cave had a growth hiatus between 6 and 7.4 ka. Whether this growth hiatus was due to dry climates is a puzzle. However, a sharp increase in the $\delta^{18}O$ from 9 ka to 8 ka may illustrate the climate turned to dry stage. In addition, the $\delta^{18}O$ values were generally heavy and reached a maximum around 4.6 ka (Fig. 12). These heavy $\delta^{18}O$ values were heavier than these in the past 700 years, not agreeing with the late Holocene $\delta^{18}O$ pattern of the Dongge record which exhibits that the heaviest $\delta^{18}O$ values appeared between 500 a and 1500 a (Wang et al., 2005). In contrast, the $\delta^{13}C$ values during 4.5–6 ka were significantly lighter than these during the past 700 years, reflecting better vegetation coverage under relatively wet climates. Similar situation exists in the 20120824-13 record during 500–4000 a (Zhao et al., 2015). The discrepancy between $\delta^{18}O$ and $\delta^{13}C$ interpretations elevates the debate about whether stalagmite $\delta^{18}O$ on millennial scale represents rainfall change (LeGrande and Schmidt, 2009; Pausata et al., 2011). Nevertheless, the Yelang Cave records support that the strongest summer monsoon with the wettest climate occurred during 9–11.5 ka over entire Holocene in the study area (An, 2000).

5.3. Climate and vegetation during the past 700 years

The upper 6 cm of YLD-15 containing transparent and pure calcite grew continuously during the past 600 years. Major features of the $\delta^{18}O$ and $\delta^{13}C$ during this period are: (1) $\delta^{18}O$ appeared strong decadal variations with decreasing amplitude from early to the present; (2) $\delta^{13}C$ increased from about −9‰ at 600a to −1.9‰ at AD 1960. This 7‰ increase in the $\delta^{13}C$ was not caused only by climate change (Fig. 12). Since the chronology uncertainty does not allow us to perform spectrum analysis, we can only use these light and heavy $\delta^{18}O$ excursions to represent wet and dry events (Fig. 9). There were 16 wet–dry episodes during the past 600 years shown by the $\delta^{18}O$ excursions. In addition, the general increasing trend of the YLD-15 $\delta^{18}O$ during

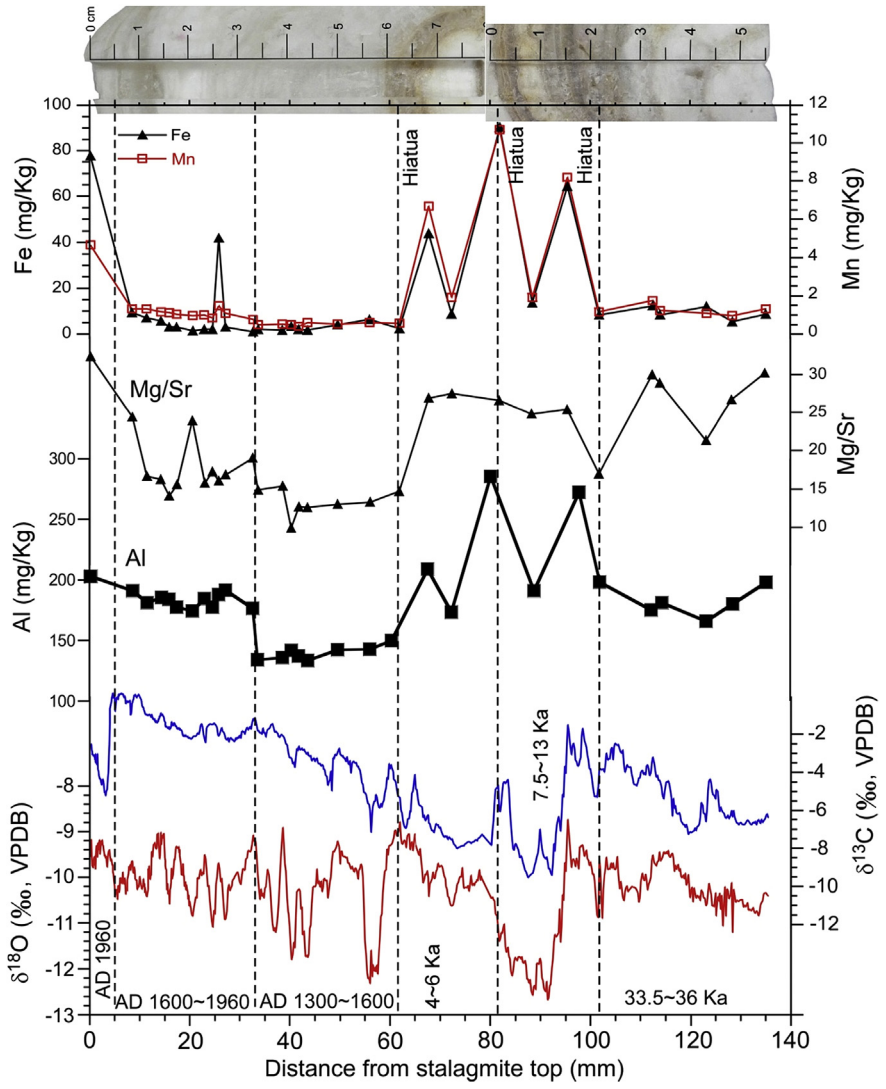

Fig. 10. Fe, Mn, Al contents and Mg/Sr rations in YLD-15 and their comparisons with the $\delta^{18}O$ and $\delta^{13}C$ records.

the past 600 years agrees with that of the 20120824-13 $\delta^{18}O$, but opposites to that of the Dongge $\delta^{18}O$ record (Zhao et al., 2015). Since the opposite trends could not be caused by age uncertainty, it is important for us to understand the reason. As discussed before, the increasing $\delta^{13}C$ trends occurred in both YLD-15 and 20120824-13 stalagmites, facilitating the $\delta^{13}C$ record as a vegetation proxy. As the population density strongly increased after Ming Dynasty (AD 1368–1644) in the study area, deforestation caused by human activity would elevate the $\delta^{13}C$ (Kuo et al., 2011; Zhao et al., 2015).

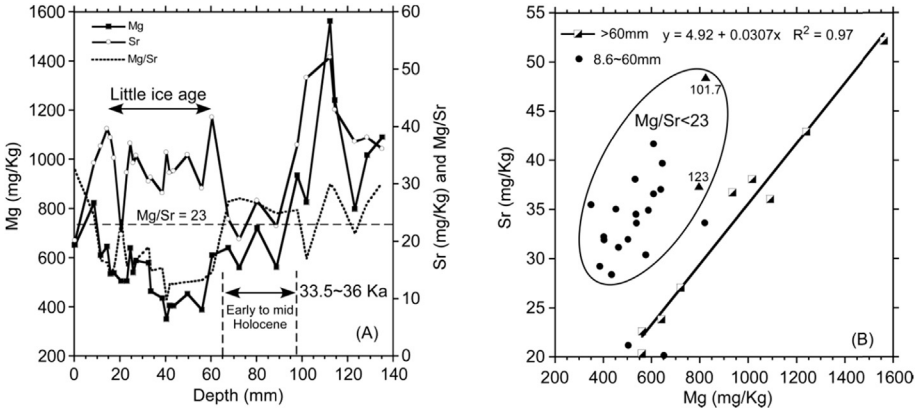

Fig. 11. (A) Mg and Sr contents and Mg/Sr ratio in YLD-15. (B) Correlation between Mg and Sr in different segments. Number beside symbol denotes the depth in mm.

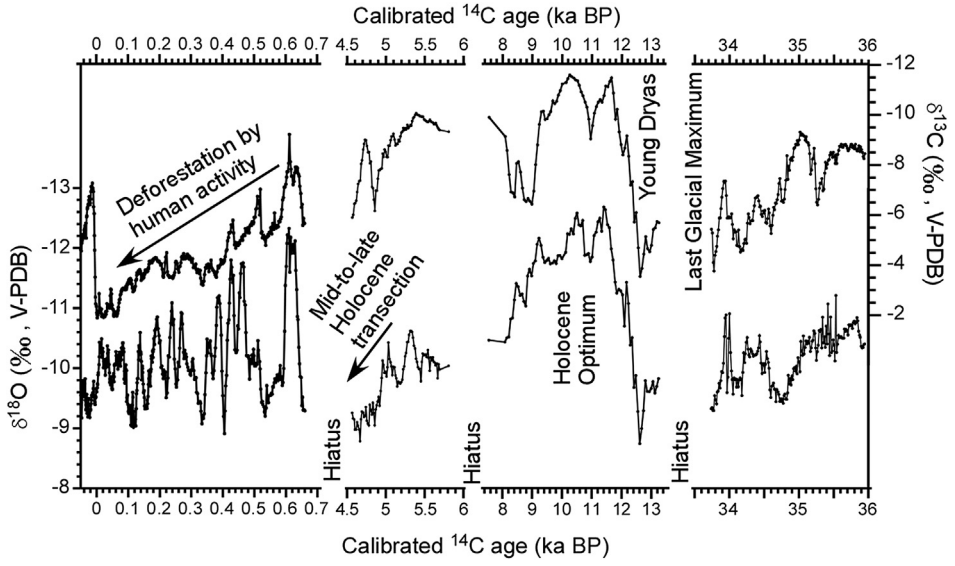

Fig. 12. The $\delta^{18}O$ and $\delta^{13}C$ records of Stalagmite YLD-15.

6. Conclusions

Results of $^{230}Th/U$, ^{210}Pb and AMS ^{14}C methods were used to build up the chronology of YLD-15 from Yelang Cave. For this low U content stalagmite, AMS ^{14}C dating results provide the best solution for chronological control whereas Stal-Age modeling approach cannot provide better chronology for YLD-15. The growth features, elemental contents and stable isotope records indicate that: (1) Three growth hiatuses occurred at 6, 8 and 9.8 cm depths, corresponding to periods of 0.7–4.5 ka, 6–7.4 ka and 13.4–33.4 ka respectively, perhaps resulted from dry climates. (2) High Fe, Mn and Al contents around the dark bands near these hiatuses demonstrate that detritus from source water and/or dust fall inside the cave contribute the elemental concentrations. (3) Very strongly positive correlation of Mg and Sr with high Mg/Sr values (>23 in this study) reflects source control on the Mg and Sr variations. Under such a circumstance, Mg/Sr is not a function of cave temperature. (4) For pure calcite without detrital influence, Mg/Sr may register changes in cave temperature because partitioning coefficient of Mg/Ca between calcite and source water is a function of temperature, so that higher Mg/Sr indicates warmer temperature.

The YLD-15 record duplicates the published record of Stalagmite 20120824-13 in terms of $\delta^{18}O$ and $\delta^{13}C$ as well as major growth hiatuses. The duplications reinforce $\delta^{18}O$ and $\delta^{13}C$ records as paleoclimate and paleovegetation proxies. The Yelang Cave records reveal that: From 33,400 to 36,000 a between Heinrich events 3 and 4, the study area was relatively cool and dry like the status of late Holocene. Vegetation was dominated by C4 plants shown by relatively heavier $\delta^{13}C$ values (−2‰ to −8‰). No growth in both stalagmites during 13.4–31 ka with heavy trending in $\delta^{18}O$ and $\delta^{13}C$ at the beginning of the hiatus may illustrate very cold and dry climates during the LGM. Cold and dry climates with poor vegetation coverage in the study area occurred during the Younger Dryas. During early Holocene, climate was the wettest and vegetation was the best between 9 and 11.5 ka shown by the lightest values of $\delta^{18}O$ and $\delta^{13}C$ in both stalagmites. These climatic and vegetation conditions were corresponding to the strongest summer monsoon under the insolation maximum throughout the Holocene. Unlike the Dongge Cave record, the Yelang Cave records indicate that climate turned to dry significantly from 9 ka to 7.5 ka. The growth hiatus between 6 and 7.4 ka in both stalagmites might be resulted from dry climates. It is important to solve the puzzle of climatic conditions in central Guizhou during the Bølling–Ållerød (BA) warming (13.5–15 ka) and the middle Holocene (6–8 ka) as one would expect warm and wet climates during these periods.

According to the $\delta^{13}C$ record of YLD-15, vegetation condition between 5 and 6 ka was better than that during the late Holocene, though heavier $\delta^{18}O$ values appeared in this interval. This case illustrates that using $\delta^{18}O$ alone to decipher climatic condition may be problematic. The climate turned to dry and vegetation started to decline after 5 ka in the study area. Shown by the 20120824-13 record, the summer monsoon strength decreased from 4 ka to 1.5 ka, but increased during the Medieval Warm Period to produce wet climates and abundant vegetation. For the past 600 years, the $\delta^{18}O$ records of both stalagmites reveal strongly decadal variations and long-term increasing (heavier) trends. The latter was opposite to the Dongge $\delta^{18}O$ record. A 6–7‰ increase in $\delta^{13}C$ of both stalagmites from around 600 yr BP (ca. −8‰) to AD 1960 (−1.9‰) should account for deforestation due to human impact.

Acknowledgements

This work was supported by the grants from NSC 102-2811-M-002-177 and MOST 103-2116-M-002-001 of Taiwan, and the funds from NSFC (41103084), 973 program (2013CB956700). $^{230}Th/U$ dating was supported by grants from Taiwan ROC MOST (104-2119-M-002-003 to C.-C.S.) and the National Taiwan University (105R7625 to C.-C.S.). Former graduate student of H.-C. Li, Mr. Zhong-Han Lee who was graduated in 2011, worked on the stalagmite for his MS thesis. We thank his contribution. The first author thanks the MOST of Taiwan for supporting her postdoc study at NTU during the past year.

References

An, Z.S., 2000. The history and variability of the East Asian paleomonsoon climate. Quaternary Science Reviews 19, 171–187.

Beck, J.W., Richards, D.A., Edwards, R.L., Silverman, B.W., Smart, P.L., Donahue, D.J., Hererra-Osterheld, S., Burr, G.S., Calsoyas, L., Jull, A.J.T., Biddulph, D., 2001. Extremely large variations in atmospheric C-14 concentration during the last glacial period. Science 292, 2453–2458.

Cheng, H., Edwards, R.L., Broecker, W.S., Denton, G.H., Kong, X.G., Wang, Y.J., Zhang, R., Wang, X.F., 2009. Ice age terminations. Science 326, 248–252.

Cheng, H., Edwards, R.L., Shen, C.-C., Polyak, V.J., Asmerom, Y., Woodhead, J., Hellstrom, J., Wang, Y.J., Kong, X.G., Spötl, C., Wang, X.F., Alexander Jr., E.C., 2013. Improvements in ^{230}Th dating, ^{230}Th and ^{234}U half-life values, and U-Th isotopic measurements by multi-collector inductively coupled plasma mass spectrometry. Earth and Planetary Science Letters 371–372, 82–91.

Chinese Academy of Meteorological Sciences (CAM), 1981. Yearly Charts of Dryness/Wetness in China for the Last 500-Year Period. SinoMap, Beijing (in Chinese), Beijing.

Chu, P.C., Li, H.-C., Fan, C.W., Chen, Y.-H., 2012. Speleothem evidence for temporal-spatial variation in East Asian summer monsoon since Medieval warm period. Journal of Quaternary Science 27 (9), 901–910.

Dorale, J.A., Liu, Z.-H., 2009. Limitations of Hendy test criteria in judging the paleoclimatic suitability of speleothems and the need for replication. Journal of Cave Karst Study 71, 73–80.

Dykoski, C.A., Edwards, R.L., Cheng, H., Yuan, D.X., Cai, Y.J., Zhang, M.L., Lin, Y.S., Qing, J.M., An, Z.S., Revenaugh, J., 2005. A high-resolution, absolute-dated Holocene and deglacial Asian monsoon record from Dongge Cave, China. Earth and Planetary Science Letters 233, 71–86.

Fairchild, I.J., Boesato, A., Tooth, A.F., Frisia, S., Hawkesworth, C.J., Huang, Y., McDermott, F., Spiro, B., 2000. Controls in trace element (Sr-Mg) compositions of carbonate cave waters: implications for speleothem climatic records. Chemical Geology 166, 255–269.

Fairchild, I.J., Smith, C.L., Baker, A., Fuller, L., Spötl, C., Mattey, D., McDermott, D., E.I.M.F, 2006. Modification and preservation of environmental signals in speleothems. Earth-Science Reviews 75, 105–153.

Fairchild, I.J., Treble, P.C., 2009. Trace elements in speleothems as records of environmental change. Quaternary Science Reviews 28, 449–468.

Fuchtbauer, H., Hardie, L.A., 1976. Experimentally determined homogeneous distribution coefficients for precipitated magnesium calcites: application to marine carbonate cements. In: Abstract in Geological Society of America, Annual Meeting, Denver, Colorado.

Gascoyne, M., 1983. Trance-element partition coefficients in the calcite-water system and their paleoclimatic significance in cave studies. Journal of Hydrology 61, 213–222.

Genty, D., Baker, A., Massault, M., Proctor, C., Gilmour, M., Pons-Branchu, E., Hamelin, B., 2001. Dead carbon in stalagmites: carbonate bedrock paleodissolution vs. ageing of soil organic matter. Implications for ^{13}C variations in speleothems. Geochimica et Cosmochimica Acta 65, 3443–3457.

Goede, A., Vogel, J.C., 1991. Trace element variations and dating of a late Pleistocene Tasmanian speleothem. Palaeogeography, Palaeoclimatology, Palaeoecology 88, 121–131.

Han, L.-Y., Li, T.-Y., Cheng, H., Edwards, R.L., Shen, C.C., Li, H.-C., Huang, C.X., Li, J.Y., Yuan, N., Wang, H.B., Zhang, T.T., Zhao, X., 2016. Potential influence of temperature changes in the southern hemisphere on the evolution of the Asian summer monsoon during the last glacial period. Quaternary International 392, 239–250. http://dx.doi.org/10.1016/j.quaint.2015.05.068.

Hemming, S.R., 2004. Heinrich events: massive late Pleistocene detritus layers of the North Atlantic and their global climate imprint. Reviews of Geophysics 42. http://dx.doi.org/10.1029/2003RG000128. RG1005H.

Hendy, C.H., 1971. The isotopic geochemistry of speleothems—I. The calculation of the effects of different modes of formation on the isotopic composition of speleothems and their applicability as paleoclimate indicators. Geochimica et Cosmochimica Acta 35, 801–824.

Hiess, J., Condon, D.J., McLean, N., Noble, S.R., 2012. ^{238}U/^{235}U systematics in terrestrial U-bearing minerals. Science 335 (6076), 1610–1614.

Hoffmann, D.L., Beck, J.W., Richards, D.A., Smart, P.L., Singarayer, J.S., Ketchmark, T., Hawkesworth, C.J., 2010. Towards radiocarbon calibration beyond 28 ka using speleothems from the Bahamas. Earth and Planetary Science Letters 289, 1–10.

Hu, C.Y., Henderson, G.M., Huang, J., Xie, S.C., Sun, Y., Johnson, K.R., 2008. Quantification of Holocene Asian monsoon rainfall from spatially separated cave records. Earth and Planetary Science Letters 266, 221–232.

Huang, Y.M., Fairchild, I.J., 2001. Partitioning of Sr and Mg into calcite under karst-analogue experimental conditions. Geochimica et Cosmochimica Acta 65, 47–62.

Jaffey, A.H., Flynn, K.F., Glendenin, L.E., Bentley, W.C., Essling, A.M., 1971. Precision measurement of half-lives and specific activities of ^{235}U and ^{238}U. Physics Reviews C 4, 1889–1906.

Johnson, K.R., Hu, C.Y., Belshaw, N.S., Henderson, G.M., 2006. Seasonal trace-element and stable-isotope variations in a Chinese speleothem: the potential for high-resolution paleomonsoon reconstruction. Earth and Planetary Science Letters 244, 394–407.

Katz, A., 1973. The interaction of magnesium with calcite during crystal growth at 25–90°C and one atmosphere. Geochimica et Cosmochimica Acta 37, 1563–1586.

Katz, A., Sass, E., Starinsky, A., 1972. Strontium behavior in the aragonite–calcite transformation: an experimental study at 40–98°C. Geochimica et Cosmochimica Acta 36, 481–496.

Kinsman, D.J.J., Holland, H.K., 1969. The co-precipitation of cations with $CaCO_3$-IV. The co-precipitation of Sr^{2+} with aragonite between 16°C and 96°C. Geochimica et Cosmochimica Acta 33, 1–17.

Ku, T.-L., Li, H.-C., 1998. Speleothems as high-resolution paleoenvironment archives: records from northeastern China. Journal of Earth System Science 107, 321–330.

Kuo, T.-S., Liu, Z.-Q., Li, H.-C., Wan, N.-J., Shen, C.-C., Ku, T.-L., 2011. Climate and environmental changes during the past millennium in central western Guizhou reflected by Stalagmite ZJD-21 record. Journal of Asian Earth Sciences 40, 1111–1120.

LeGrande, A.N., Schmidt, G.A., 2009. Sources of Holocene variability of oxygen isotopes in paleoclimate archives. Climate of the Past 5, 441–455.

Li, H.-C., Ku, T.-L., Chen, W.-J., Jiao, W.-Q., Zhao, S.-S., Chen, T.-M., Li, T.-Y., 1996. Isotope studies of Shihua Cave, Beijing – II: radiocarbon dating and age correction of stalagmite. Seismology and Geology 18, 329–338.

Li, H.-C., Ku, T.-L., Stott, L.D., Chen, W.J., 1998. Applications of interannual-resolution stable isotope records of speleothem: climatic changes in Beijing and Tianjin, China during the past 500 years — the δ^{18}O record. Science in China 41, 362–368.

Li, H.-C., Lee, Z.-H., Wan, N.-J., Shen, C.-C., Li, T.Y., Yuan, D.X., Chen, Y.H., 2011a. Interpretations of δ^{18}O and δ^{13}C in aragonite stalagmites from Furong Cave, Chongqing, China: a 2000-year record of monsoonal climate. Journal of Asia Earth Sciences 40, 1121–1130.

Li, H.-C., Zhao, M., Tsai, C.-H., Mii, H.-S., Wei, K.-Y., 2015. The first high-resolution stalagmite record from Taiwan: climate and environmental changes during the past 1300 years. Journal of Asian Earth Science 114, 574–587.

Li, J.Y., Li, H.-C., Liu, Z.Q., Yuan, D.X., He, X., Wang, R.M., 2006. Geochemistry features and Mg/Sr ratios of water and speleothem samples from caves in central western Guizhou, China. Carsologica Sinica 25, 177–186 (in Chinese).

Li, T.-Y., Shen, C.-C., Huang, L.-J., Jiang, X.-Y., Yang, X.-L., Mii, H.S., Lee, S.Y., Lo, L., 2014. Stalagmite-inferred variability of the Asian summer monsoon during the penultimate glacial-interglacial period. Climate of the Past 10 (3), 1211–1219.

Li, T.-Y., Shen, C.-C., Li, H.-C., Li, J.-J., Chiang, H.-W., Song, S.-R., Yuan, D.-X., Lin, Chris D.-J., Gao, P., Zhou, L.-P., Wang, J.-L., Ye, M.-Y., Tang, L.-L., 2011b. Oxygen and carbon isotopic systematics of aragonite speleothems and water in Furong Cave, Chongqing, China. Geochimica et Cosmochimica Acta 75, 4140–4156.

Ma, Z.B., Cheng, H., Tan, M., Edwards, R.L., Li, H.-C., You, C.F., Duan, W.H., Wang, X., Kelly, M., 2012. Timing and structure of the Younger Dryas event in northern China. Quaternary Science Reviews 41, 83–93.

Ma, Z.-B., Li, H.-C., Xia, M., Ku, T.-L., Peng, Z.-C., Chen, Y.-S., Zhang, Z.-F., 2002. Paleotemperature changes over the past 3000 years in eastern Beijing, China: a reconstruction based on Mg/Sr records in a stalagmite. Chinese Science Bulletin 48 (4), 395–400.

Olesik, J.W., 1991. Elemental analysis using ICP-OES and ICP/MS. Analytical Chemistry 63 (1), 12A–21A.

Oster, J.L., Montañez, I.P., Guilderson, T.P., Sharp, W.D., Banner, J.L., 2010. Modeling speleothem δ^{13}C variability in a central Sierra Nevada cave using ^{14}C and ^{87}Sr/^{86}Sr. Geochimica et Cosmochimica Acta 74, 5228–5242.

Paulsen, D.E., Li, H.-C., Ku, T.-L., 2003. Climate variability in central China over the last 1270 years revealed by high-resolution stalagmite records. Quaternary Science Reviews 22, 691–701.

Pausata, F.S.R., Battisti, D.S., Nisancioglu, K.H., Bitz, C.M., 2011. Chinese stalagmite δ^{18}O controlled by changes in the Indian monsoon during a simulated Heinrich event. Nature Geoscience 4, 474–480.

Qian, W., Lin, X., 2005. Regional trends in recent precipitation indices in China. Meteorology and Atmospheric Physics 90, 193–207.

Scholz, D., Hoffmann, D.L., 2011. StalAge — an algorithm designed for construction of speleothem age models. Quaternary Geochronology 6, 369–382.

Shen, C.-C., Cheng, H., Edwards, R.L., Moran, S.B., Edmonds, H.N., Hoff, J.A., Thomas, R.B., 2003. Measurement of attogram quantities of ^{231}Pa in dissolved and particulate fractions of seawater by isotope dilution thermal ionization mass spectroscopy. Analytical Chemistry 75, 1075–1079.

Shen, C.-C., Wu, C.-C., Cheng, H., Edwards, R.L., Hsieh, Y.-T., Gallet, S., Chang, C.-C., Li, T.-Y., Lam, D.D., Kano, A., Hori, M., Spötl, C., 2012. High-precision and high-resolution carbonate ^{230}Th dating by MC-ICP-MS with SEM protocols. Geochimica et Cosmochimica Acta 99, 71–86.

Southon, J., Noronha, A.L., Cheng, H., Edwards, R.L., Wang, Y.J., 2012. A high-resolution record of atmospheric ^{14}C based on Hulu Cave speleothem H82. Quaternary Science Reviews 33, 32–41.

Stuiver, M., Reimer, P.J., 1986. A computer program for radiocarbon age calibration. Radiocarbon 28 (2B), 1022–1030.

Stuiver, M., Reimer, P.J., 1993. Extended ^{14}C data base and revised CALIB 3.0 ^{14}C age calibration program. Radiocarbon 35, 215–230.

Tan, M., 2009. Circulation effect: climatic significance of the short term variability of the oxygen isotopes in stalagmites from monsoonal China—dialogue between paleoclimate records and modern climate research. Quaternary Sciences 29, 851–862 (In Chinese).

Wan, N.-J., Chung, W.-L., Li, H.-C., Lin, H.L., Shen, C.-C., Ku, T.-L., Yuan, D.X., Zhang, M.L., Lin, Y.S., 2011a. The comparison of speleothem δ^{18}O records from Eastern China with solar insolation, ice core and marine records: similarities and discrepancies on different time scales. Journal of Asia Earth Sciences 40, 1151–1163.

Wan, N.-J., Li, H.-C., Liu, Z.Q., Yuan, D.X., 2011b. Spatial variations of monsoonal rain in eastern China: instrumental, historic and speleothem records. Journal of Asia Earth Sciences 40, 1139–1150.

Wang, Y.J., Cheng, H., Edwards, R.L., An, Z.S., Wu, J.Y., Shen, C.-C., Dorale, J.A., 2001. A high-resolution absolute-dated late Pleistocene monsoon record from Hulu Cave, China. Science 294, 2345–2348.

Wang, Y.J., Cheng, H., Edwards, R.L., He, Y., Kong, X., An, Z.S., Wu, J., Kelly, M.J., Dykoski, C.A., Li, X., 2005. The Holocene Asian monsoon: links to solar changes and north Atlantic climate. Science 308, 854–857.

Wang, Y.J., Cheng, H., Edwards, R.L., Kong, X., Shao, X., Chen, S., Wu, J., Jiang, X., Wang, X., An, Z.S., 2008. Millennial- and orbital-scale changes in the East Asian monsoon over the past 224,000 years. Nature 451, 1090–1093.

Yin, J.J., Yuan, D.X., Li, H.-C., Cheng, H., Li, T.Y., Edwards, R.L., Lin, Y.S., Qin, J.M., Tang, W., Zhao, Z.Y., Mii, H.S., 2014. Variation in the Asian monsoon intensity and dry-wet condition since the little Ice Age in central China revealed by an aragonite stalagmite. Climate of The Past 10, 1803–1816.

Yuan, D.X., Cheng, H., Edwards, R.L., Dykoski, C.A., Kelly, M.J., Zhang, M.L., Qing, J.M., Lin, Y.S., Wang, Y.J., Wu, J., Dorale, J.A., An, Z.S., Cai, Y.J., 2004. Timing, duration, and transition of the last interglacial Asian monsoon. Science 304, 575–578.

Zhang, D.E., Li, H.-C., Ku, T.-L., Lu, L.H., 2010. On linking climate to Chinese dynastic change: spatial and temporal variations of monsoonal rain. Chinese Science Bulletin 55, 77–83.

Zhang, D.E., Li, X.Q., Liang, Y.Y., 2003. Continuation (1992–2000) of the yearly charts of dryness/wetness in China for the last 500 years period. Journal of Applied Meteorological Science 14, 379–388 (in Chinese with English abstract).

Zhang, H.-L., Yu, K.-F., Zhao, J.-X., Feng, Y.-X., Lin, Y.-S., Zhou, W., Liu, G.-H., 2013. East Asian summer monsoon variations in the past 12.5 ka: high-resolution $\delta^{18}O$ record from a precisely dated aragonite stalagmite in central China. Journal of Asian Earth Science 73, 162–175.

Zhao, M., Li, H.-C., Liu, Z.-H., Mii, H.-S., Sun, H.-S., Shen, C.-C., 2015. Changes in climate and vegetation of central Guizhou in southwest China since the last glacial reflected by stalagmite records from Yelang Cave. Journal of Asian Earth 114, 549–561.